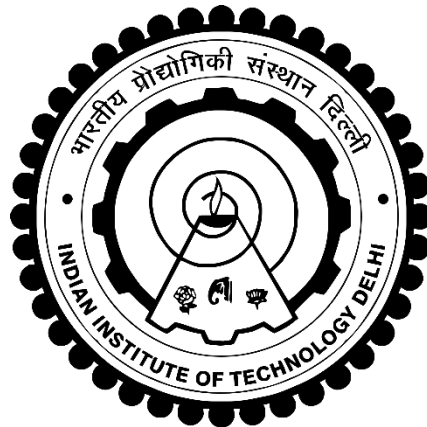


STUDY OF SUPERCONDUCTING PROPERTIES OF YBCO NANOCOMPOSITES AND STEP EDGE JOSEPHSON JUNCTION BASED DEVICES

Rajni

(2020PHZ8785)



**DEPARTMENT OF PHYSICS
INDIAN INSTITUTE OF TECHNOLOGY DELHI**

JULY 2025

© Indian Institute of Technology Delhi (IITD), New Delhi, 2025

STUDY OF SUPERCONDUCTING PROPERTIES OF YBCO NANOCOMPOSITES AND STEP EDGE JOSEPHSON JUNCTION BASED DEVICES

by

RAJNI

Department of Physics

Submitted

in fulfilment of requirements of the degree of Doctor of Philosophy

to the



DEPARTMENT OF PHYSICS

INDIAN INSTITUTE OF TECHNOLOGY DELHI

JULY 2025

Dedicated
to
My Family

CERTIFICATE

This is to certify that the thesis entitled “**Study of Superconducting Properties of YBCO Nanocomposites and Step Edge Josephson Junction Based Devices**”, being submitted by **Ms. Rajni** to the **Department of Physics, Indian Institute of Technology, Delhi**, is worthy of consideration for the award of the degree of **Doctor of Philosophy** and is a record of the original bonafide research work carried out by her under my guidance and supervision. She has fulfilled all the criteria for the submission of the thesis, which is in my opinion has reached the necessary standard.

The results contained in this thesis have not been submitted, in part or full, to any other university or institute for the award of any degree/diploma.



Prof. Neeraj Khare

Department of Physics

Indian Institute of Technology Delhi

Hauz Khas, New Delhi-110016,

India

ACKNOWLEDGEMENTS

First and foremost, I wish to express my profound gratitude to the Almighty God and The Pitra Dev, whose boundless grace and unwavering strength have been the guiding light throughout my journey. It is through His divine blessings that I have cultivated the patience, courage, and determination needed to overcome the many challenges encountered along the way.

I am profoundly grateful to my research supervisor, Prof. Neeraj Khare, for his invaluable guidance, expertise, and mentorship. His unwavering support has been the cornerstone of this thesis, shaping not only the trajectory of my work but also influencing my personal and professional growth. His insightful advice, constructive critiques, and constant encouragement have inspired me to persevere and strive for excellence. I am truly indebted to him for his generosity with time, his patience with my learning curve, and his dedication to fostering my academic development.

My heartfelt thanks also extend to the esteemed members of the student research committee, Prof. Pankaj Srivastava, Prof. Sujeet Chaudhary, and Prof. Samaresh Das, for their constructive feedback, thoughtful questions, and professional advice. Their critical evaluations and insightful suggestions challenged me to approach my research with greater clarity and rigor, and I deeply appreciate their time and expertise.

I also wish to acknowledge the Nanoscale Research Facility (NRF), Central Research Facility (CRF), Department of Physics, and all the technical staff at IIT Delhi for their invaluable assistance and provision of characterization facilities throughout my research. Their support has been vital to the successful execution of this work.

Additionally, I am sincerely grateful to the Council of Scientific and Industrial Research (CSIR), India, for the financial support provided through the Junior Research Fellowship (JRF) and Senior

Research Fellowship (SRF). Their contribution has been instrumental in enabling me to focus on my research endeavors.

I extend my sincerest gratitude to my colleagues at the Nano Functional Oxides and Superconductivity Laboratory (NFOSL), including Dr. Mohd. Faraz, Prof. Alok Kumar Jha, Dr. Deepanshu Sharma, Dr. Satyendra Prakash Pal, Dr. Rohit Kumar, Dr. Simrjit Singh, Dr. Sandeep Munjal, Dr. Kannan U. M, Dr. Huidrom Hemojit Singh, Dr. Nitish Yadav, Dr. Dheeraj Kumar, Dr. Mamta Dahiya, Dr. Amish Kumar Gautam, Dr. Mohit Khosya, Dr. Birendra Kumar, Dr. Gaurav Sharma, Mrs. Abhilasha Chouksey, Dr. Arun Mondal, Dr. Manoj Singh, Mr. Aman Sharma, Mr. Gaurav Kumar, Mr. Sandeep Kumar, Ms. Sarita Mittal. The support and contributions of the team have been instrumental in establishing an effective and supportive working environment within the laboratory. I am thankful to Mr. Amit Gupta and Mr. Arjun Singh as lab assistants.

I want to thank Dr. Mamta Dahiya, Dr. Mohd. Faraz and Mr. Sandeep Kumar, for generously sharing their experiences, knowledge, constant motivation, and all the discussions, which have been particularly beneficial to me.

I extend my profound love and gratitude to my family, whose unwavering support has been the foundation of every achievement I have attained. To my late grandparents, Mr. Dhoom Singh Kandari and Mrs. Ramdei Devi; my late father, Mr. Nagendra Singh Kandari, and my mother, Mrs. Rajeshwari Devi; my late uncle, Mr. Jagdish Singh, and my aunt, Mrs. Urmila Devi your blessings, prayers, and sacrifices have shaped my path, and this accomplishment is as much yours as it is mine. To my brothers, Mr. Rajesh Kandari, Mr. Sanwar Singh, and Mr. Harshvardhan Singh, my sister, Ms. Sangeeta, and my sister-in-law, Mrs. Shakuntala Kandari your unwavering faith in me and continued encouragement have been instrumental in my perseverance. A special

place in my heart is reserved for my beloved niece, Ms. Tripty, who fills our lives with joy and hope. I am also deeply grateful to my cousins and extended family for your unwavering support, reminding me of the true value of generosity and humanity.

Furthermore, I cherish my friends Sonika Singh, Naina Kushwaha, Simranjeet Kaur, Shivani Kumawat, Arun Mondal, Manoj Singh, Neelam, Ankita Rawat, Arunesh Singh, Prabal Dweep Khanikar, Gazal Gupta, Sakshi Garg, Monika Rana, Nisha Rawat, Kuldeep Kunwar, Pankaj Rawat, Ganesh Sati, Sahin Alam, Nakul Kumar, Lalit Pandey, Nanhe Kumar Gupta, Jay Krishna Anand, Shailendra Singh, Sonali Rai, Deepika Singh, Himasmita, Sarita Mittal, Sandeep Kumar, Neha Jain, Mohit Bhatt, Ekta Yadav, Anupriya Tiwari, Shreyashi Sinha, Subi Nath, Pratyusha Thakur, Puspita Chanda for their unwavering support through trials and triumphs. Your encouragement, understanding, and belief in my capabilities have been invaluable. Thank you for uplifting my spirits during challenging times and celebrating the milestones along this journey with me.

Last but not the least, I express my profound gratitude to all my teachers, from childhood to the present, who have guided me with wisdom and nurtured my curiosity. Their invaluable support has shaped my academic journey and personal growth.

Rajni

ABSTRACT

High-temperature superconductors (HTS) are a special class of materials that exhibit zero electrical resistance and perfect diamagnetism at relatively high temperatures, typically above the boiling point of liquid nitrogen (77 K). One of the most extensively researched HTS materials is $\text{YBa}_2\text{Cu}_3\text{O}_{7-x}$ (YBCO), which is known for its remarkable superconducting properties. However, practical applications of YBCO have major challenges: (i) for bulk superconductors, the sharp decline in critical current density (J_c) in the presence of external magnetic fields, and (ii) for thin film devices such as Josephson junctions, the low values of characteristic voltage (which is the product of critical current I_c and normal state resistance R_n) also known as I_cR_n product. In order to address the first issue, artificial pinning centers are introduced in the YBCO matrix to improve flux pinning and slow down the reduction of J_c . For the second challenge, step edge Josephson junctions emerge as a preferred fabrication method due to their flexibility in junction positioning and relatively simple fabrication process. Through precise control of fabrication parameters, key device characteristics such as I_c , R_n , and I_cR_n product can be optimized. Additionally, implementing multiple junctions in an array configuration enhances the overall I_cR_n product, presenting a promising pathway for advancing superconducting device performance.

In order to investigate the effect of the magnetic nature of nano additive flux pinning, magnetic NiO nanoparticles are introduced as artificial pinning centers in the bulk YBCO matrix. YBCO and its nanocomposite samples (YBCO-NiO) are synthesized by adding magnetic NiO nanoparticles utilizing the solid state reaction method. X-ray diffraction of the nanocomposite samples confirmed that all retained the orthorhombic structure of YBCO. The NiO nanoparticles display ferromagnetic behavior with a saturation magnetization of approximately 0.85 emu/g, remanence around 0.057 emu/g, and a coercive field of about 89 Oe. The critical temperature (T_c)

is 91 K for pure YBCO, and its value changes to 90 K for the YBCO- 0.1 wt% NiO and 87 K for the YBCO- 0.2 wt% NiO nanocomposites. Magnetization vs. applied magnetic field loops at 20 K and 60 K show a larger hysteresis loop for the YBCO- 0.1 wt% NiO nanocomposite compared to pure YBCO, indicating stronger pinning. By using Bean's critical state model on the hysteresis data, critical current density (J_c) is determined. The improvement factor (f) in J_c , calculated for applied fields up to 5 T and all temperatures, is found to be greater than 1, confirming the enhancement in pinning for the YBCO- NiO nanocomposite sample. In the case of magnetic nano additives, two mechanisms improve the pinning: first, the incorporation of nanoparticles introduces structural defects in YBCO matrix, and second, additional pinning is achieved through magnetic interaction with vortices. At higher applied fields, however, the inter-vortex magnetic interactions weaken, and the enhanced pinning is predominantly due to structural defects introduced in YBCO due to the presence of NiO.

However, YBCO step edge Josephson junctions on SrTiO₃ (STO) substrates are fabricated and characterized for superconducting device applications, and the resistively shunted junction (RSJ) model fitting is done using PSCAN2 software. A well defined step with a height of 450 nm and a step angle of 18° created on the STO substrate using photolithography followed by ion beam etching. A microbridge of 100 μm length and 10 μm width is fabricated across the YBCO deposited step edge STO substrate and characterized by resistance vs. temperature and current vs. voltage measurements. Parameters such as critical temperature, T_c , critical currents, I_c , and normal state resistance (R_n) are measured at different temperatures. Resistively shunted junction (RSJ) model fitting using PSCAN2 reveals the overdamped behavior of the junction, which is attributed to the presence of normal conducting channels in the microbridge, leading to additional rounding in the experimental data.

A systematic investigation of the impact of YBCO film thickness (t) relative to the substrate step height (h) on the junction parameters as I_c , R_n , and $I_c R_n$ product of the YBCO step edge Josephson junction is analyzed. A step edge on STO substrates is fabricated, such as the step height (h) is 450 nm. YBCO films, with thicknesses tuned via controlling the laser shots, are deposited on the step edged STO substrate. Atomic force microscopy confirmed t/h ratios of ~ 0.4 , 0.7 , and 1.2 . YBCO microbridges $\sim 100 \times 10 \mu\text{m}^2$ are fabricated across the step edge, and electrical measurements yielded critical temperatures of around 82, 85, and 88 K, respectively. The $I_c R_n$ products, at 70 K, are 2.06, 2.76, and 0.43 mV for respective t/h ratios of 0.4, 0.7 and 1.2. Fitting the critical current I_c vs. reduced temperature ($1-T/T_c$) indicates that the junctions behave as a superconductor–normal metal–superconductor (SNS) type. These results highlight the critical influence of the t/h ratio on junction performance, offering a pathway to optimize the YBCO based Josephson junctions.

Achieving the higher value of characteristic voltage, $I_c R_n$, is possible by fabricating an array of junctions. An array of four junctions is designed using CleWin5 software and fabricated an array of four junctions on YBCO film deposited on a $5 \times 5 \text{ mm}^2$ step edge etched STO substrate by second-level lithography and ion beam milling process. Electrical measurements of individual junctions, namely J1, J2, J3, and J4, show nearly identical values of critical currents I_c and normal state resistances R_n , confirming the quality and uniformity of the fabricated junctions. At 70 K, a single junction possessed an I_c of $\sim 530 \mu\text{A}$ and R_n of 5Ω , while arrays of two, three, and four junctions showed progressively increasing R_n values of 7, 9.7, and 12.5Ω , with I_c values of ~ 510 , 500, and $490 \mu\text{A}$, respectively. Notably, the $I_c R_n$ product for single and four junctions are ~ 2.7 and 6 mV increasing with the number of junctions, demonstrating the feasibility of this approach for enhancing device performance.

सार

उच्च तापमान अतिचालक (HTS), पदार्थों का एक विशेष वर्ग है जो अपेक्षाकृत उच्च तापमान पर, आमतौर पर तरल नाइट्रोजन के क्वथनांक (77 K) से ऊपर शून्य विद्युत प्रतिरोध और पूर्ण प्रतिचुंबकीयता प्रदर्शित करते हैं। इन HTS पदार्थों में $YBa_2Cu_3O_{7-x}$ (YBCO) सबसे अधिक अध्ययन किया गया पदार्थ है, जो अपनी उत्कृष्ट अतिचालक विशेषताओं के लिए जाना जाता है। हालाँकि, YBCO के व्यावहारिक अनुप्रयोगों में कई प्रमुख चुनौतियाँ हैं: (i) समष्टि अतिचालक के लिए, बाहरी चुंबकीय क्षेत्रों की उपस्थिति में क्रांतिक धारा घनत्व (J_c) में तेज गिरावट, और (ii) जोसेफसन जंक्शनों में $I_c R_n$ गुणनफल का निम्न मान। पहले मुद्दे को हल करने के लिए, YBCO मैट्रिक्स में कृत्रिम पिनिंग केंद्रों को जोड़ा जाता है ताकि फ्लक्स पिनिंग में सुधार किया जा सके और J_c की कमी को धीमा किया जा सके। दूसरे चुनौती के लिए, स्टेप एज जोसेफसन जंक्शन पसंदीदा निर्माण विधि के रूप में उभरते हैं, क्योंकि इनमें जंक्शन की स्थिति को लचीले ढंग से नियंत्रित करने और अपेक्षाकृत सरल निर्माण प्रक्रिया की सुविधा होती है। निर्माण परिमाणों की सटीक नियंत्रण के माध्यम से, प्रमुख उपकरण विशेषताओं जैसे I_c , R_n , और $I_c R_n$ गुणनफल को अनुकूलित किया जा सकता है। इसके अतिरिक्त, एक श्रृंखला विन्यास में बहु-जंक्शन को लागू करने से कुल $I_c R_n$ गुणनफल को बढ़ाया जाता है, जो सुपरकंडक्टिंग उपकरणों के प्रदर्शन को आगे बढ़ाने के लिए एक आशाजनक मार्ग प्रस्तुत करता है।

नैनो संयोजित पदार्थ के चुंबकीय स्वभाव के फ्लक्स पिनिंग पर प्रभाव की जांच करने के लिए, समष्टि YBCO मैट्रिक्स में कृत्रिम पिनिंग केंद्रों के रूप में चुंबकीय NiO नैनोकणों को जोड़ा गया है। YBCO और इसके नैनोकंपोजिट नमूने (YBCO-NiO) को ठोस-अवस्था अभिक्रिया विधि से चुंबकीय NiO नैनोकणों को जोड़कर संश्लेषित किया गया। एक्स-रे विवर्तन ने पुष्टि की कि सभी नमूनों ने ऑर्थोरोम्बिक संरचना को बनाए रखा। NiO नैनोकणों ने लगभग 0.85 emu/g का संतृप्त चुंबकत्व, लगभग 0.057 emu/g का अवशिष्ट चुंबकत्व और लगभग 89 Oe का प्रतिरोधी क्षेत्र दर्शाया, जो इनकी लौहचुंबकीय प्रकृति को दर्शाता है। YBCO, 91 K का क्रांतिक तापमान (T_c) दर्शाता है, जबकि 0.1 wt.% नैनोकॉम्पोजिट के लिए यह 90 K और 0.2 wt.% के लिए 87 K है। 0.2 wt.% नमूने में T_c में उल्लेखनीय गिरावट NiO नैनोकणों के एकत्रित होने को दर्शाती है। 20 K और 60 K पर चुंबकीय क्षेत्र के विरुद्ध चुंबकत्व पाश दर्शाते हैं, कि YBCO-0.1 wt% NiO नैनोकॉम्पोजिट के लिए शैथिल्य पाश, शुद्ध YBCO की तुलना में ज्यादा है,

जो पिनिंग का संकेत देता है। 5 T तक के सभी तापमानों पर J_c में सुधार कारक (f) एक से अधिक पाया गया, जिससे YBCO नैनोकॉम्पोजिट में पिनिंग के सुधार की पुष्टि होती है। चुंबकीय नैनो योगज में, पिनिंग को बेहतर बनाने के दो प्रमुख क्रियाविधि कार्य करती हैं: पहली, नैनोकणों की उपस्थिति से संरचनात्मक दोष उत्पन्न होते हैं; और दूसरी, भँवर (vortices) के साथ चुंबकीय अंतःक्रिया के माध्यम से अतिरिक्त पिनिंग प्राप्त होती है। हालाँकि, उच्च चुंबकीय क्षेत्रों में भँवर-अंतःक्रिया कमजोर हो जाती है, जिससे पिनिंग मुख्यतः संरचनात्मक दोषों पर निर्भर हो जाती है।

YBCO स्टेप एज जोसेफसन जंक्शन्स को SrTiO_3 (STO) सब्सट्रेट्स पर तैयार किया गया है और अतिचालक उपकरण अनुप्रयोगों के लिए उनका परीक्षण किया गया है। STO सब्सट्रेट पर 450 नैनोमीटर की ऊँचाई और 18° के स्टेप कोण के साथ एक स्टेप तैयार किया गया, जिसका निर्माण फोटोलिथोग्राफी और उसके बाद आयन बीम एचिंग द्वारा किया गया। YBCO निक्षिप्त स्टेप एज STO सब्सट्रेट पर 100 माइक्रोमीटर लंबा और 10 माइक्रोमीटर चौड़ा माइक्रोब्रिज तैयार किया गया और उसका परीक्षण प्रतिरोध बनाम तापमान और धारा बनाम विभव मापों के माध्यम से किया गया। विभिन्न तापमानों पर क्रांतिक तापमान (T_c) और क्रांतिक धारा (I_c) जैसे परिमाण मापे गए। PSCAN2 का उपयोग करते हुए प्रतिरोधक रूप से शंट किया जंक्शन (RSJ) मॉडल की फिटिंग से जंक्शन का अति-अवमंदित व्यवहार स्पष्ट हुआ, जो माइक्रोब्रिज में सामान्य चालक चैनलों की उपस्थिति के कारण था, जिसके कारण प्रयोगात्मक आंकड़ों में अतिरिक्त गोलाई आई।

YBCO फ़िल्म की मोटाई (t) और सब्सट्रेट स्टेप ऊँचाई (h) के बीच के संबंध का व्यवस्थित अध्ययन किया गया है, और YBCO स्टेप एज जोसेफसन जंक्शन के परिमाण जैसे I_c , R_n और $I_c R_n$ गुणनफल पर इसके प्रभाव का विश्लेषण किया गया है। YBCO फ़िल्में, जिनकी मोटाई को लेजर शॉट के माध्यम से नियंत्रित किया गया। परमाणु बल सूक्ष्मदर्शी ने t/h अनुपातों की पुष्टि की, जो लगभग 0.4, 0.7 और 1.2, और क्रांतिक तापमान 82, 85, और 88 K हैं। 70 K पर, $I_c R_n$ गुणनफल, क्रमशः t/h अनुपात 0.4, 0.7 और 1.2 के लिए 2.06, 2.76 और 0.43 mV हैं। I_c और तापमान ($1-T/T_c$) के बीच के संबंध को फिट करने से यह संकेत मिलता है कि जंक्शन्स एक अतिचालक-सामान्य धातु- अतिचालक (SNS) प्रकार के रूप में व्यवहार करते हैं। ये परिणाम t/h अनुपात के जंक्शन प्रदर्शन पर महत्वपूर्ण प्रभाव को उजागर करते हैं, जो YBCO आधारित जोसेफसन जंक्शन्स को अनुकूलित करने का एक मार्ग प्रदान करते हैं।

$I_c R_n$, का उच्च मान प्राप्त करना, जंक्शन की एक श्रृंखला बनाकर संभव है। चार जंक्शनों की एक श्रृंखला CleWin5 सॉफ्टवेयर में डिज़ाइन की गई और YBCO निक्षिप्त स्टेप एज STO सब्सट्रेट पर द्वितीय-स्तरीय लिथोग्राफी और एचिंग प्रक्रिया के माध्यम से निर्मित किया गया। जंक्शनों J1, J2, J3 और J4 के विद्युत मापन से I_c और R_n के लगभग समान मान प्राप्त हुए, जो निर्मित जंक्शनों की गुणवत्ता और एकरूपता की पुष्टि करता है। विशेष रूप से, 70 K पर एक एकल जंक्शन में लगभग 530 μA का I_c और 5 Ω का R_n पाया गया, जबकि दो, तीन और चार जंक्शनों की श्रृंखला के R_n मान क्रमशः 7, 9.7 और 12.5 Ω और I_c मान क्रमशः लगभग 510, 500, और 490 μA थे। ध्यान देने योग्य बात यह है कि एकल और चार जंक्शनों के लिए $I_c R_n$ गुणनफल क्रमशः लगभग 2.7 mV और 6 mV था, जो जंक्शनों की संख्या बढ़ने के साथ बढ़ता गया। यह दृष्टिकोण उपकरण के प्रदर्शन को बेहतर बनाने के लिए एक प्रभावी रणनीति साबित होती है।

TABLE OF CONTENTS

CERTIFICATE.....	i
ACKNOWLEDGEMENTS	ii
ABSTRACT.....	v
TABLE OF CONTENTS	xi
LIST OF FIGURES	xviii
LIST OF TABLES.....	xxii
Chapter 1- Introduction	1
1.1 Overview.....	1
1.2 Basics of Superconductivity	3
1.2.1 Zero Electrical Resistance.....	3
1.2.2 The Meissner Ochsensfeld Effect.....	3
1.2.3 Flux Quantization.....	5
1.3 Types of Superconductors.....	6
1.3.1 Type I Superconductors	7
1.3.2 Type II Superconductors	7
1.4 High Temperature Superconductor (HTS)	8
1.4.1 YBa ₂ Cu ₃ O _{7-x} (YBCO) Superconductor	9
1.4.2 Flux Pinning.....	11
1.4.2.1 Natural and Artificial Pinning Centers.....	13
1.4.2.2 Magnetic and Non-Magnetic Pinning Centers.....	13
1.5 YBCO Thin Films and Devices	14

1.5.1	Josephson Effect	15
1.5.1.1	The DC Josephson Effect.....	16
1.5.1.2	The AC Josephson Effect.....	16
1.5.2	Types of HTS Josephson Junctions.....	17
1.5.3	Resistively Shunted Junction (RSJ) Model	19
1.5.4	Array of Junctions.....	20
1.6	Motivation of the Work.....	21
1.7	Objectives of the Present Thesis.....	22
1.7.1	Organization of the Thesis.....	22
1.7.1.1	Chapter 1: Introduction.....	23
1.7.1.2	Chapter 2: Experimental Methods and Characterization Techniques	23
1.7.1.3	Chapter 3: Effect of Magnetic NiO Nanoparticles on the Pinning Properties of YBCO Superconductor	24
1.7.1.4	Chapter 4: Fabrication and RSJ Modeling of YBCO Step Edge Josephson Junction	24
1.7.1.5	Chapter 5: Effect of Film Thickness to Step Height Ratio on the Performance of the YBCO Step Edge Josephson Junction	25
1.7.1.6	Chapter 6: Fabrication and Study of the Series Array of YBCO Step Edge Josephson Junctions	26
1.7.1.7	Chapter 7: Conclusions and Future Scope.....	26
	References.....	27
	Chapter 2- Experimental Methods and Characterization Techniques	31
2.1	Introduction.....	31

2.2	Synthesis of YBCO, Nanostructured Materials and Composites	31
2.2.1	Auto Combustion Method	32
2.2.2	Solid State Reaction Method	33
2.2.3	YBCO Target for PLD Technique	35
2.3	Fabrication Techniques Used for Josephson Junction	35
2.3.1	Dicing Saw: Substrate Cutting Tool	35
2.3.2	Lithography Techniques	37
2.3.2.1	Fabrication of Photomask	37
2.3.2.2	Mask Aligner: Lithography Technique	38
2.3.3	Etching Techniques.....	40
2.3.3.1	Ar Ion Beam: Dry Etching Technique	41
2.3.4	Film Deposition Technique.....	42
2.3.4.1	Pulsed Laser Deposition Technique	43
2.4	Characterization Techniques	45
2.4.1	X- Ray Diffraction	45
2.4.2	Field Emission Scanning Election Microscopy	47
2.4.3	Atomic Force Microscopy	49
2.5	Measurement Systems	51
2.5.1	Electrical Transport Measurements	51
2.5.1.1	Helium Closed Cycle Cryocooler	51
2.5.2	Magnetic Measurements	54
2.5.2.1	Physical Properties Measurement System	54
	References.....	56

Chapter 3- Effect of Magnetic NiO Nanoparticles on the Pinning Properties of YBCO Superconductor	58
3.1 Introduction.....	58
3.2 Experimental Section	60
3.2.1 Synthesis of NiO Nanoparticles.....	60
3.2.2 Synthesis of YBCO	60
3.2.3 Synthesis of YBCO- NiO Nanocomposite Samples.....	61
3.2.4 Structural and Morphological Studies	62
3.2.5 Electrical Measurements	62
3.2.6 Magnetic Measurements	62
3.3 Results and Discussion	63
3.3.1 Structural and Morphological Study of NiO.....	63
3.3.2 Magnetic Study of NiO Nanoparticles.....	64
3.3.3 Structural Analysis of YBCO and Nanocomposite Samples.....	66
3.3.4 Elemental Analysis of YBCO and Nanocomposite Samples	67
3.3.5 Electrical Transport Measurements	68
3.3.6 Magnetic Measurements	69
3.4 Conclusions.....	74
References	76
Chapter 4- Fabrication and RSJ Modeling of YBCO Step Edge Josephson Junction	79
4.1 Introduction.....	79
4.2 Experimental Section	80
4.2.1 Fabrication of Step on STO Substrate.....	81
4.2.1.1 Substrate Cutting Using a Dicing Saw Tool	81
4.2.1.2 First Level Lithography on STO Substrate	82

4.2.1.3 Etching of STO Substrate to Form a Step	83
4.2.2 YBCO Film Deposition on Step Etched STO	83
4.2.3 Fabrication of Microbridge	84
4.2.3.1 Second Level Lithography for the Fabrication of Microbridge	84
4.2.3.2 Etching of YBCO Film to Form a Microbridge	85
4.3 Results and Discussion	85
4.3.1 Surface Studies	85
4.3.1.1 Atomic Force Microscopy Study	85
4.3.1.2 X-Ray Diffraction Analysis of Deposited Film	86
4.3.1.3 Optical Microscopic Analysis	87
4.3.1.4 Field Emission Scanning Electron Microscopy Analysis	87
4.3.2 Electrical Transport Measurements of YBCO Film.....	88
4.3.2.1 Resistivity vs. Temperature Measurements of YBCO Film.....	88
4.3.3 Electrical Transport Measurements of Step Edge Junction.....	89
4.3.3.1 Resistivity vs. Temperature Measurements.....	90
4.3.3.2 Current vs. Voltage Measurements	90
4.4 PSCAN2 Software	92
4.4.1 Resistively Shunted Junction Model Fitting.....	92
4.5 Conclusions.....	94
References	95
Chapter 5- Effect of Film Thickness to Step Height Ratio on the Performance of the YBCO Step Edge Josephson Junction	97
5.1 Introduction.....	97
5.2 Experimental Section	98
5.2.1 Fabrication of YBCO Step Edge Junctions (SEJs)	98

5.3	Results and Discussion	100
5.3.1	AFM and FESEM Analysis	100
5.3.2	Electrical Transport Studies of Step Edge Junctions	101
5.3.2.1	Resistivity vs. Temperature Measurements	101
5.3.2.2	Current vs. Voltage Measurements.....	102
5.4	Conclusions.....	106
	References	107
Chapter 6- Fabrication and Study of the Series Array of YBCO Step Edge Josephson Junctions		109
6.1	Introduction.....	109
6.2	Experimental Section	110
6.2.1	Fabrication of Step Edge Junction	110
6.2.1.1	Designing of Array Pattern using CleWin5 Software.....	111
6.2.1.2	Fabrication of the Array of YBCO Step Edge Junctions.....	111
6.3	Results and Discussion	112
6.3.1	AFM and SEM Surface Analysis.....	112
6.3.2	Electrical Transport Studies	113
6.3.2.1	Resistivity vs. Temperature Measurements	113
6.3.2.2	Current vs. Voltage Measurements.....	114
6.4	Conclusions.....	119
	References	121
Chapter 7- Conclusions and Future Scope		123
7.1	Conclusions of the Thesis	123
7.1.1	Effect of Magnetic Nickel Oxide NiO Nanoparticles on the Pinning Properties of YBCO Superconductor.....	123

7.1.2	Fabrication and RSJ Modeling of YBCO Step Edge Josephson Junction	124
7.1.3	Study of the Effect of the Film Thickness to Step Height Ratio on the YBCO Step Edge Josephson Junction	125
7.1.4	Fabrication and Study of the Series Array of YBCO Step Edge Josephson Junctions	126
7.2	Future Scope of the Thesis.....	126
	List of Publications	128
	Author's Biodata.....	131

LIST OF FIGURES

Figure 1.1	Change in resistance of Mercury (Hg) with respect to temperature [2].	2
Figure 1.2	Behavior of superconductors in magnetic field for $T > T_c$ and $T < T_c$ [6].	4
Figure 1.3	Flux quantization in (a) hollow superconducting cylinder, and (b) superconducting ring [3].	6
Figure 1.4	Magnetization vs. applied field behavior of (a) type I and (b) type II superconductors [6].	7
Figure 1.5	Schematic diagram of YBCO unit cell for (a) $x = 1$ and (b) $x = 0$ [5].	9
Figure 1.6	(a) Flux pinning in the mixed state and (b) critical current density vs. magnetic field behavior of type II superconductor [20].	12
Figure 1.7	(a) Schematic diagram and (b) current vs. voltage characteristic of Josephson junction [14].	15
Figure 1.8	Different types of HTS Josephson junctions, (a) bicrystal, (b) step edge, (c) step edge SNS, and (d) ramp edge junction [7].	18
Figure 1.9	Schematic diagram of resistively shunted junction (RSJ) model of Josephson junction.	19
Figure 2.1	Schematic diagram for the auto combustion synthesis method.	32
Figure 2.2	(a) Morter pestle, (b) hydraulic press, and (c) tube furnace used for the synthesis of YBCO via solid state reaction method.	34
Figure 2.3	Image of the (a) 1-inch diameter pellet press dies and (b) YBCO target mounted on target holder.	35
Figure 2.4	The image of experimental dicing saw tool.	36
Figure 2.5	Image of (a) CleWin5 layout software and (b) Chrome photomask.	38
Figure 2.6	Schematic diagram of the photolithography process of mask aligner.	39
Figure 2.7	Experimental setup of mask aligner photolithography technique.	40
Figure 2.8	Schematic diagram showing the working process of dry etching.	41
Figure 2.9	Experimental setup of Ar ion beam etching technique and zoomed view inside the chamber.	42
Figure 2.10	Schematic diagram of pulsed laser deposition technique.	44
Figure 2.11	Experimental setup of pulsed laser deposition technique.	45

Figure 2.12	(a) Schematic diagram of working principle and (b) schematic representation of experimental setup of XRD measurement system.	46
Figure 2.13	Schematic diagram of electron beam interaction with the specimen [18].	47
Figure 2.14	Schematic diagram showing the working of the field emission scanning electron microscope [18].	49
Figure 2.15	Schematic diagram of the working principle of atomic force microscope [19].	50
Figure 2.16	Schematic diagram of experimental setup used for electrical transport measurements.	52
Figure 2.17	Experimental setup of Helium cryocooler and the zoomed view of OFHC sample holder.	53
Figure 2.18	Experimental setup of physical properties measurement system.	55
Figure 3.1	Schematic diagram for the synthesis of Nickel oxide nanoparticles via auto combustion method.	60
Figure 3.2	Schematic diagram of the synthesis process of YBCO and YBCO-NiO nanocomposite samples.	61
Figure 3.3	XRD pattern of Nickel oxide nanoparticles.	63
Figure 3.4	(a) FESEM image, (b) particle size distribution, and (c) TEM image of synthesized NiO nanoparticles.	64
Figure 3.5	Variation of (a) magnetization with applied field, (b) magnetization with temperature, and (c) $-d(M_{FC}-M_{ZFC})/dT$ versus temperature curve of synthesized NiO nanoparticles.	65
Figure 3.6	XRD spectra of YBCO, YBCO-0.1wt% NiO, and YBCO-0.2wt% NiO nanocomposite samples.	67
Figure 3.7	SEM images of (a) YBCO, (b) YBCO- 0.1wt% NiO, EDX analysis of (c) YBCO, and (d) YBCO- 0.1wt% NiO nanocomposites.	68
Figure 3.8	The variation of electrical resistivity (ρ) with temperature (T) measurement of YBCO, YBCO 0.1wt% NiO, and YBCO-0.2wt% NiO nanocomposite samples.	69
Figure 3.9	Variation of magnetization (M) with magnetic field (H) at (a) 20 K and (b) 60 K of YBCO and its nanocomposite sample.	70
Figure 3.10	Variation of critical current density (J_c) with applied field (H) of YBCO and YBCO-0.1wt% NiO nanocomposite sample at (a) 20 K, (b) 60 K, and (c) improvement factor (f) with applied fields graph at 20 K, 40 K, and 60 K.	72

Figure 3.11	Variation of pinning force with applied field measurement at (a) 20 K, (b) 60 K of YBCO and YBCO-0.1wt% NiO nanocomposite sample, and (c) improvement factor (g') in flux pinning with applied fields at 20 K, and 60 K.	73
Figure 4.1	Schematic diagram of the fabrication process of YBCO step edge Josephson junction on STO substrate.	81
Figure 4.2	Schematic diagram of the photolithography process of the patterning a step on STO substrate.	82
Figure 4.3	Image of the second level lithography, shows the alignment of the microbridge in a mask (top) across the step (bottom) on YBCO deposited step edge STO substrate.	84
Figure 4.4	(a) AFM image and (b) step profile of etched STO substrate.	85
Figure 4.5	XRD pattern of the YBCO film deposited on STO substrate.	86
Figure 4.6	Optical microscopic image of the YBCO microbridge across the step etched STO substrate.	87
Figure 4.7	FESEM image of (a) YBCO film deposited over the step etched on STO substrate, (b) SEM micrograph of the fabricated YBCO microbridge, and (c) zoomed view of YBCO microbridge.	88
Figure 4.8	Resistance vs. temperature plot of YBCO film deposited on STO substrate.	89
Figure 4.9	Schematic diagram used for the electrical transport measurements of YBCO step edge junction.	89
Figure 4.10	Resistance vs. temperature plot of the YBCO step edge junction.	90
Figure 4.11	Plots of (a) current vs. voltage measurements and (b) critical current vs. temperature plot of YBCO step edge junction.	91
Figure 4.12	Experiment and RSJ fitted I-V curves of YBCO step edge junction.	93
Figure 5.1	Schematic diagram of the fabrication process of YBCO step edge junction (a) patterning of step, (b) etching and film deposition, (c) patterning of the junction, and (d) second time etching.	99
Figure 5.2	(a) AFM image (top view) of step etched STO substrate, FESEM image of (b) YBCO microbridge, from (c) upper (unetched) region, and (d) lower (etched) region of YBCO film.	100
Figure 5.3	Resistance vs. temperature curves of the fabricated devices for t/h ratios (a) 0.4, (b) 0.7, and (c) 1.2, respectively.	102

Figure 5.4	The current vs. voltage curves of the fabricated step edge junction devices at different temperatures having t/h ratios as (a) 0.4, (b) 0.7, and (c) 1.2.	103
Figure 5.5	Plot of (a) I_c and R_n with temperature, and (b) product of $I_c R_n$ with temperature of YBCO step junction devices having t/h ratio of 0.4, 0.7, and 1.2, respectively	104
Figure 5.6	Experimental variation of I_c with $(1-T/T_c)$ for the step edge junction having a t/h ratio as (a) 0.4, (b) 0.7, and (c) 1.2, respectively. The solid lines are the best fitted lines as per equation (5.1).	105
Figure 6.1	Schematic diagram of the process followed to fabricate the array of step edge junctions.	110
Figure 6.2	Design of the soft mask of (a) array of four junctions and (b) zoomed image of the single junction.	111
Figure 6.3	(a) AFM micrograph of the step etched STO substrate, (b) SEM micrograph of a fabricated array of four junctions, and (c) zoomed SEM micrograph of single step edge junction J3.	112
Figure 6.4	(a) Schematic representation for electrical measurements and (b) resistance vs. temperature measurement of the array configuration, inset: critical temperatures of the single junctions J1, J2, J3, and J4.	114
Figure 6.5	Current vs. voltage curves of the number of the single junction array of two, three, and four junctions of the array at 70 K.	115
Figure 6.6	(a) Current vs. voltage curves and (b) spread in the values of critical current, I_c , and normal state resistance, R_n , for each of the individual junction (J1, J2, J3, and J4) at 70 K.	116
Figure 6.7	Current vs. voltage curves of a number of junctions at different temperatures for (a) a single junction, the array of (b) two junctions, (c) three junctions, and (d) four junctions.	117
Figure 6.8	Variation of (a) normal state resistance, R_n and (b) $I_c R_n$ product with respect to the number of junctions at 70 K.	118
Figure 6.9	Critical current, I_c , vs. $(1-T/T_c)$ curve of YBCO step edge junction, where solid lines are fitted curve to equation (6.1).	119

LIST OF TABLES

Table 1.1	Typical parameters of a stoichiometric $\text{YBa}_2\text{Cu}_3\text{O}_7$ structure [6].	10
Table 1.2	Various substrates used for the growth of YBCO film [41].	14

NOMENCLATURE

List of Abbreviations

YBCO	Yttrium Barium Copper Oxide
STO	Strontium Titanate
NiO	Nickle Oxide
JJ	Josephson Junction
HTS	High Temperature Superconductor
LTS	Low Temperature Superconductor
SEJ	Step Edge Junction
RSJ	Resistively Shunted Junction
BCS	Bardeen-Cooper-Schrieffer
PSCAN	Portable Superconducting Circuit Analyzer
GB	Grain Boundary
SQUID	Superconducting Quantum Interference Device
SQIFs	Single Flux Quantum Interference Filters
XRD	X-Ray Diffraction
SEM	Scanning Electron Microscopy
TEM	Transmission Electron Microscopy
PPMS	Physical Properties Measurement System
AFM	Atomic Force Microscopy
IBE	Ion Beam Etching
PLD	Pulsed Laser Deposition

List of Symbols

R	Resistance
T	Temperature
I	Current
V	Voltage
T_c	Critical Temperature
I_c	Critical Current
J_c	Critical Current Density
B_a	External Applied Field
Φ_0	Flux Quantization
H_c	Critical Field
H_{c1}	Lower Critical Field
H_{c2}	Upper Critical Field
F_P	Pinning Force
F_L	Lorentz Force
ξ	Coherence Length
λ	Penetration Depth
R_n	Normal State Resistance
C	Capacitance
h	Plank's Constant
e	Electric Charge
ϕ	Phase Difference

ρ	Resistivity
M	Magnetization
α	Step Angle
t	Film Thickness
h	Step Height